High $Q\times f$ values of Zn-Ni co-modified $LiMg_{0.9}Zn_{0.1-x}Ni_xPO_4$ microwave dielectric ceramics for 5G/6G LTCC modules

Shuai Li[a], Chen Li[a], Minmin Mao[a], Kaixin Song[a,*],Yaseen Iqbal[b], Amir Khesro[c], Sinan S. Faouri[d], Zhilun Lu[e], Bing Liu[a], Shikuan Sun[f], Dawei Wang[g,*]

[a]*College of Electronics Information, Hangzhou Dianzi University, Hangzhou, 310018, China*

[b]*Department of Physics, University of Peshawar, 25120, KP, Pakistan*

[c]*Department of Physics, Abdul Wali Khan University, Mardan, 23200, Pakistan*

[d]*Mechanical and Industrial Engineering Department, Applied Science Private University, 11931, Amman-Jordan*

[e]*School of Engineering and the Built Environment, Edinburgh Napier University, Edinburgh, EH10 5DT, United Kingdom*

[f]*School of Material Science and Energy Engineering, Foshan University, Foshan, Guangdong, 528000, China*

[g]*Shenzhen Institute of Advanced Electronic Materials, Shenzhen Institute of Advanced Technology, Chinese Academy of Sciences, Shenzhen, 518055, China*

Abstract: In this work, Zn-Ni co-modified $LiMg_{0.9}Zn_{0.1-x}Ni_xPO_4$ (x=0-0.1) microwave dielectric ceramics were fabricated using a solid oxide synthesis route. Rietveld refinement of the XRD data revealed that all ceramic samples have formed a single phase with olivine structure. SEM images showed that the samples have a dense microstructure, that agrees with the measured relative density of 97.73%. Based on the complex chemical bond theory, Raman and infrared reflectance spectra, we postulate that ε_r is mainly affected by the ionic polarizability, lattice and bond energy, while P-O bond plays a decisive role in $Q\times f$ and τ_f value. Optimum properties of $Q\times f$ = 153,500GHz, ε_r ~ 7.13 and τ_f ~ -59ppm/°C were achieved for the composition $LiMg_{0.9}Zn_{0.06}Ni_{0.04}PO_4$ sintered at 875 °C for 2h. This set of properties makes these

ceramics an excellent candidate for LTCC, wave-guide filters and antennas for 5G/6G communication applications.

Keywords: $LiMgPO_4$; Microwave dielectric ceramic; 5G/6G communication

1. Introduction

Rapid development of microwave communication technology demands miniaturization, integration, and multifunctionality in electronic devices. Compared to other materials, ceramics have a wider range of relative permittivity and better mechanical stability making them a material of choice for filters, duplexers, resonators, dielectric antennas and other related devices [1-6]. Recent developments in 5G/6G communication technology have affirmed the pivotal role of low temperature co-fired ceramics (LTCC) technology in integrated antennas [7-8]. LTCCs are characterized by low dielectric constant (ε_r), high quality factor ($Q\times f$) and near-zero temperature coefficient of resonant frequency (τ_f), which are desirable for many industries including aerospace, military, communication, and automotive electronics [9-10]. Owing to its importance, the development of microwave dielectric ceramics with excellent performance and low sintering temperature (lower than melting point of Ag, 961℃) have been a subject of intensive research in recent times [11,12].

Lithium phosphate microwave dielectric ceramics such as $LiNiPO_4$, $LiZnPO_4$, $LiMnPO_4$, $LiMgPO_4$, have been widely studied for microwave applications, because of their low sintering temperature and low ε_r [13-20]. In 2010, Thomas et al. initially found

that $LiMgPO_4$ ceramics sintered at 950°C yield excellent microwave dielectric properties with ε_r = 6.6, $Q\times f$ = 79,100 GHz and τ_f = -55 ppm/°C [21]. Subsequently, they reported improved microwave dielectric properties of $LiMg_{0.9}Zn_{0.1}PO_4$ ceramics (ε_r = 6.7, $Q\times f$ = 99,700 GHz and τ_f = -62 ppm/°C) and that of $LiMg_{0.9}Zn_{0.1}PO_4$ ceramics with TiO_2 (ε_r = 10, $Q\times f$ = 26,900 GHz and τ_f = +1.2 ppm/°C) [22]. In 2014, Dong et al. found that Ni^{2+} and Co^{2+} ions substitution enhanced the microwave dielectric properties of $LiMgPO_4$ ceramics with reported values of ε_r = 6.91, $Q\times f$ = 98,600 GHz and τ_f = -55.3 ppm/°C for $LiMg_{0.95}Ni_{0.05}PO_4$ and ε_r = 6.97, $Q\times f$ = 111,200 GHz and τ_f = -53.8 ppm/°C for $LiMg_{0.95}Co_{0.05}PO_4$ respectively [23,24]. In 2019, Zhang et al. reported that the ceramics $LiMg_{0.96}Mn_{0.04}PO_4$ and $LiMg_{0.94}Ca_{0.06}PO_4$ yielded excellent microwave dielectric properties. The set of values for both are ε_r = 6.54, $Q\times f$ = 84,343 GHz and τ_f = -44.9 ppm/°C and ε_r = 6.96, $Q \times f$ = 88,968 GHz and τ_f = -44.7 ppm/°C, respectively [25]. It should be noted that most of the previous research has focused on improving the performance $LiMgPO_4$ via single element doping. However, it is rare to study the synergistic tuning effect of two or more elements on the crystal structure and microwave performance of $LiMgPO_4$.

Herein, Zn-Ni co-modified $LiMgPO_4$ ($LiMg_{0.9}Zn_{0.1-x}Ni_xPO_4$) microwave dielectric ceramics were prepared as a function of different Zn/Ni ratios listed in Table S1. And the effect of Zn/Ni ratio on the phase structure, microstructure and microwave dielectric properties were studied in detail.

2. Experimental

Using high purity Li_2CO_3 (99.99%, Aladdin), $4MgCO_3\cdot Mg(OH)_2\cdot 5H_2O$ (99%,

Sinopharm Reagent), NiO (99.99%, Aladdin), ZnO (99.99%, Aladdin) and $NH_4H_2PO_4$ (99%, Aladdin) as raw material, $LiMg_{0.9}Zn_{0.1-x}Ni_xPO_4$ (x=0, 0.02, 0.04, 0.05, 0.06, 0.08, 0.1) ceramics were prepared by a traditional solid-state reaction method. The powders were dried and then weighed according to stoichiometric ratios followed by ball-milling for 12 hours, using alcohol as medium. The slurry was dried at 80°C for 24 hours. which was followed by calcination at 800°C for 4 hours. After that, the obtained powder was ball-milled and dried again. The dried powder was manually ground, with polyvinyl alcohol solution (5wt%) as a binder, and finally pressed into cylinders with a diameter of 10 mm under a pressure of 100MPa. The green pellets were sintered in range of 850°C-950°C for 2 hours.

Bulk densities were measured by the Archimedes principle [26,27]. Crystalline structure of the sintered samples was confirmed by the X-ray diffraction (XRD, D5000-HTXRD) using Cu Kα radiation at room temperature. The detailed structure refinements were obtained by a Fullprof program. The sintered samples were polished and thermally etched at a temperature of 50°C lower than the sintering temperature for 1 h, and then the microstructure of the ceramics was observed by a scanning electron microscope (SEM, Magellan 400 FESEM, HITACHI, Japan). The room-temperature Raman spectra were recorded by a Raman spectrometer (Renishaw, UK) in the wavenumber from 200 cm^{-1} to 1200 cm^{-1}. The microwave dielectric properties of the samples were tested by a Hakki–Coleman resonator method and an Agilent E8362B network analyzer (Agilent, USA) in a resonant cavity. The τ_f values of the ceramics were measured using a temperature chamber and calculated by equation (1) [12,28]:

$$\tau_f = \frac{f(85°C) - f(25°C)}{(85-25) \times f(25°C)} \times 10^6 \, (ppm/°C) \quad (1)$$

3. Results and discussion

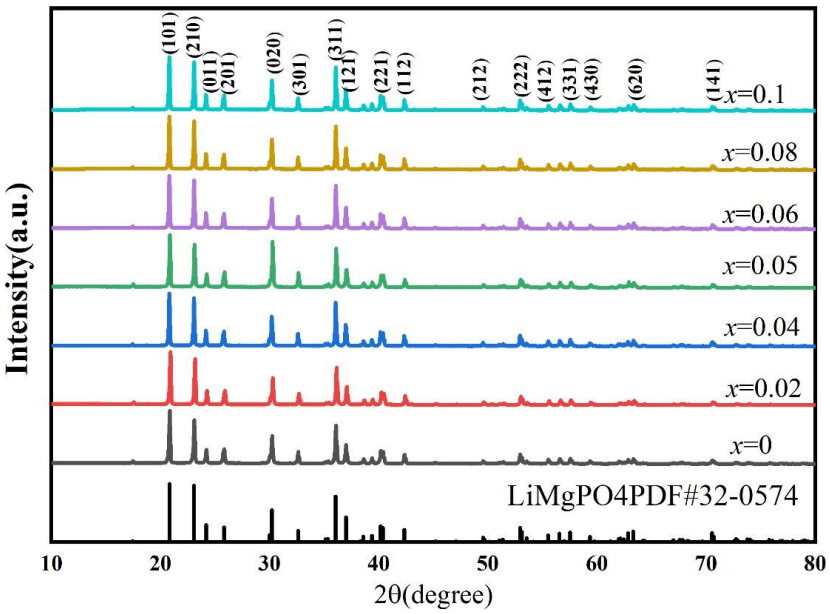

Fig. 1 XRD patterns of $LiMg_{0.9}Zn_{0.1-x}Ni_xPO_4$ ($0 \leq x \leq 0.1$).

Fig. 1 shows the XRD patterns of $LiMg_{0.9}Zn_{0.1-x}Ni_xPO_4$ ($0 \leq x \leq 0.1$), that matches well with the standard PDF card #32-0574 for $LiMgPO_4$ with space group *Pnma* and orthorhombic olivine structure. No secondary phases are detected within the XRD limit. Fig. 2(a) and Table S2 further provide the Rietveld refinement profiles of XRD data and corresponding crystal structure parameters of $LiMg_{0.9}Zn_{1-x}Ni_xPO_4$ ($0 \leq x \leq 0.1$) ceramics. For Zn^{2+}/Ni^{2+} is 3/2, the average complex ionic radii of Zn^{2+}-Ni^{2+} are calculated in Table S1. The average ionic radius of (Zn^{2+}-Ni^{2+}) at x = 0.04 is equal to that of Mg^{2+} (0.72Å), hence $LiMg_{0.9}Zn_{0.06}Ni_{0.04}PO_4$ looks like $LiMgPO_4$. Fig. 2(b) depicts that Li, Mg and P exist in the form of six coordinated octahedron ([LiO_6], [MgO_6]) and four coordinated tetrahedron ([PO_4]) respectively. The [PO_4] tetrahedron passes through [LiO_6] octahedron and [MgO_6] octahedron relate to each other to form

a spatial three-dimensional skeleton structure.

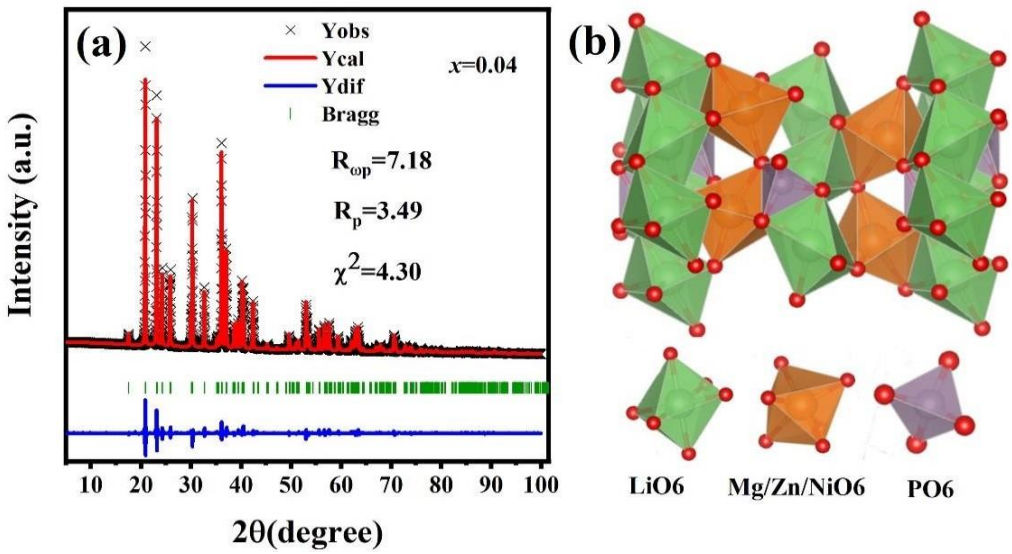

Fig. 2 (a) Schematic diagram of full spectrum fitting results of $LiMg_{0.9}Zn_{0.06}Ni_{0.04}PO_4$ ceramics, and (b) the crystal structure of $LiMgPO_4$ ceramics.

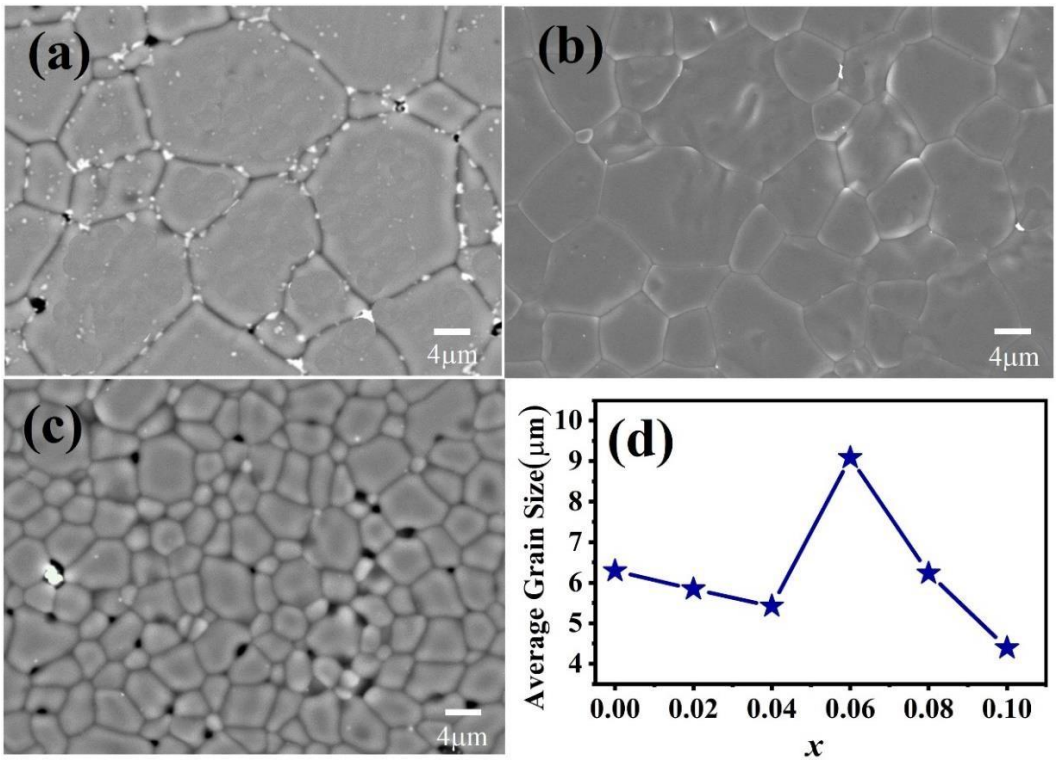

Fig. 3 SEM images of $LiMg_{0.9}Zn_{0.1-x}Ni_xPO_4$ ($0 \leq x \leq 0.1$): (a) x=0; (b) x=0.04;(c) x=0.1; (d) average grain size trend.

Fig. 3 shows the SEM images of $LiMg_{0.9}Zn_{0.1-x}Ni_xPO_4$ ($0 \leq x \leq 0.1$) ceramics. With the decrease in Zn^{2+}/Ni^{2+} ratio, the average grain size first decreases and then increases. Poor microwave performance at x=0 can be linked to high porosity, evident in the SEM image (Fig. 3a). At x = 0.04, the microstructure is greatly improved, and pores are eliminated to a great extent (Fig. 3b). This improvement in microstructure and density can be attribute to similar ionic radii of Mg^{2+} and dopants, which is also reflected in the excellent properties shown by these compositions.

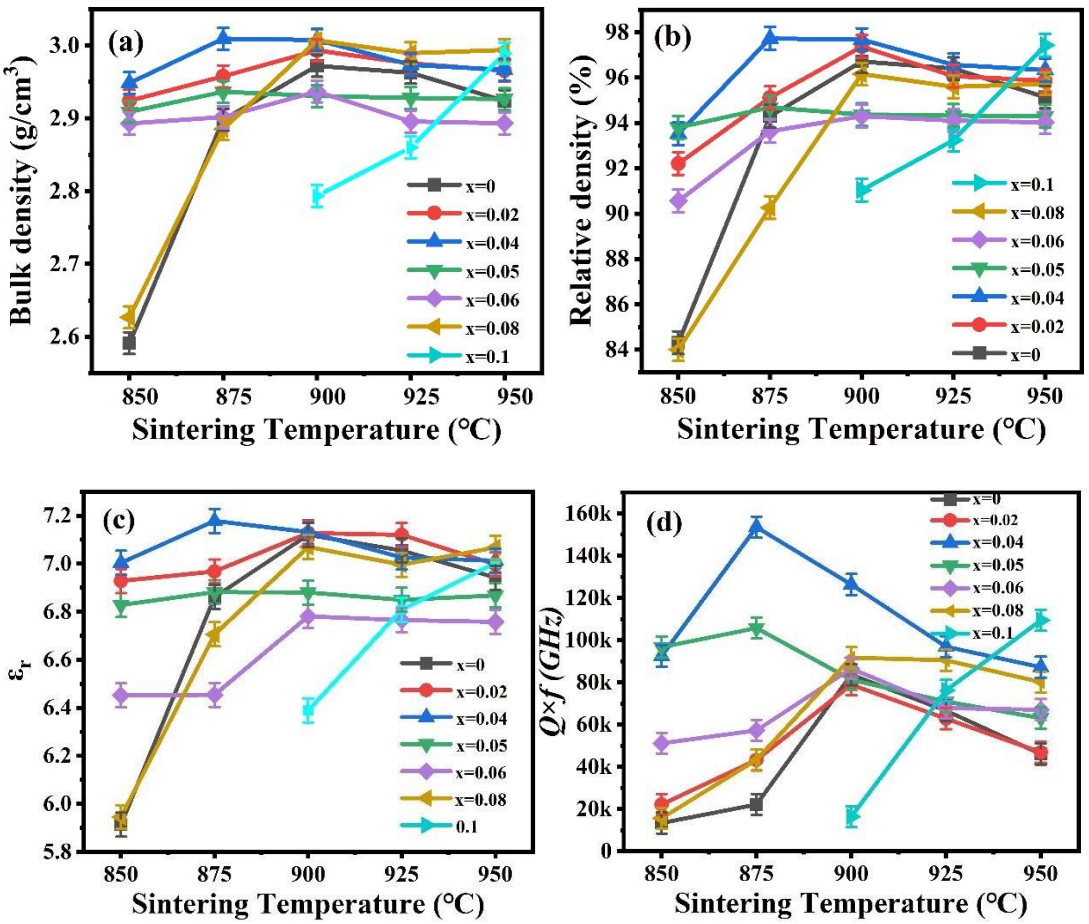

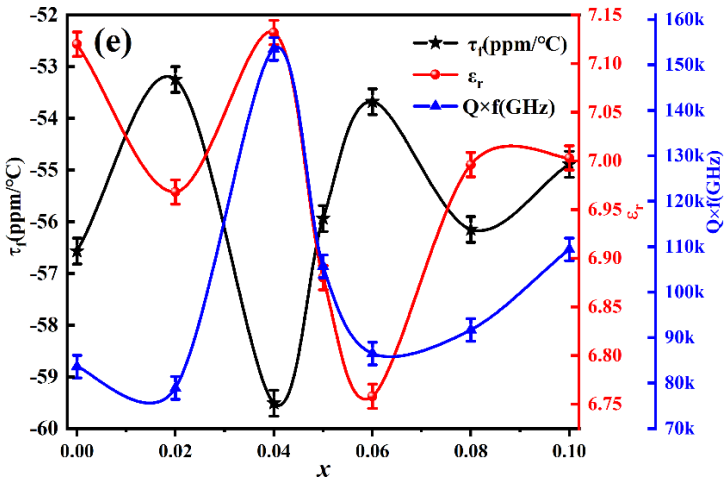

Fig. 4 Density and microwave dielectric properties of $LiMg_{0.9}Zn_{0.1-x}Ni_xPO_4$ as a function of sintering temperature: (a) bulk density; (b) relative density; (c) ε_r; (d) $Q\times f$. (e) τ_f, ε_r and $Q\times f$ values as a function of x at their optimized sintering temperature.

The bulk density ρ of $LiMg_{0.9}Zn_{0.1-x}Ni_xPO_4$ as a function of sintering temperature is plot in Fig. 4(a). The variation of Zn^{2+}/Ni^{2+} ratio does not affect ρ within the sintering range of 850°C-950°C, which indicates that the ρ of different Zn^{2+}/Ni^{2+} ratios is almost independent of sintering temperature. At x = 0.04, the maximum ρ of 3.009g/cm^3 is achieved at 875°C, corresponding to a ρ_r of 97.73%, as shown in Fig. 4(b). The varying trend of ε_r across samples is plotted in Fig. 4(c), which is commensurate with the changing ρ_r, indicating that ρ_r is the main influencing factor of ε_r. With the increase in Ni^{2+} concentration, the $Q\times f$ values rise to a maximum of 153,500GHz at x=0.04, but then start decreasing with further increase in Ni^{2+} concentration as shown in Fig 4(d). Fig S1, compares $Q\times f$ of $LiMgPO_4$ with different doped compositions. It can be observed that the co-substitution of Zn^{2+}/Ni^{2+} has greatly improves the $Q\times f$ value. It is to be noted that the Ni^{2+} substitution has a very little effect on both ε_r and τ_f as shown in Fig. 4(e)

The effect of ρ_r on ε_r and other intrinsic factors of ceramics can be understood from the set of relations, including the Clausius-Mossotti equation [29-31] given in formula (2). The total ionic polarizability is obtained by superposition of ionic polarizability of different elements α_D, from which theorical dielectric constant ε_{theo} can be obtained. The relative dielectric constant measured actually ε_{obs} and ε_{theo} can be linked after porosity P corrected dielectric constant ε_c. The effect of different Ni^{2+} doping on the dielectric properties of $LiMg_{0.9}Zn_{0.1-x}Ni_xPO_4$ ceramics was investigated by comparing ε_{theo}, ε_{obs} and ε_c. The relationship between ε_c, P and ε_{obs} is shown in Equation (3) and Equation (4):

$$\alpha_D = \frac{V_m(\varepsilon_{theo} - 1)}{b(\varepsilon_{theo} + 2)} \tag{2}$$

$$\mathrm{P} = 1 - \rho_r \tag{3}$$

$$\varepsilon_c = \varepsilon_{obs}(1 + 1.5\mathrm{P}) \tag{4}$$

where V_m is the unit cell volume of the dielectric ceramic, and b is a constant $\frac{4}{3}\pi$.

From Fig. S2, it can be found that with the increase of Ni doping, ε_{theo} decreases, while ε_c, ε_{theo} have shown a similar zigzag trend. ε_{obs} mainly depends on ρ_r, combined with Fig. 4 (b), we can see obvious fluctuation on the ε_{obs} curve. Therefore, with the increase of x, ε_r of $LiMg_{0.9}Zn_{0.1-x}Ni_xPO_4$ ceramics decreases gradually.

Phillips-Van Vechten-Levine (P–V–L) theory analyzes ceramic materials from the micro level [32-34]. It needs to refine the structure to obtain the unit cell parameters of the corresponding materials and the valence bond length of the corresponding atoms. Through these parameters, the contribution of ionic and covalent bond to lattice energy can be calculated, thus the polarization of atoms on the micro scale can be linked to the

microwave performance on the macro scale. By importing the refined parameters into Diamond software, it can be found that Li(Mg/Zn/Ni)PO_4 has three different cations Li^+, (Mg/Zn/Ni) $^{2+}$ and P^{5+}, and three different anions O(1), O(2) and O(3). These ions combine to form the following three types of chemical bonds: Li-O(1), Li-O(2) and Li-O(3) corresponding to Li^+ ions, and (Mg/Zn/Ni)-O(1), (Mg/Zn/Ni)-O(2), (Mg/Zn/Ni)-$O(3)^1$ and (Mg/Zn/Ni)-$O(3)^2$ corresponding to (Mg/Zn/Ni) $^{2+}$, the corresponding P^{5+} ions are P-O(1), P-O(2) and P-O(3), respectively. The structure of $LiMg_{0.9}Zn_{0.1-x}Ni_xPO_4$ was analyzed by complex chemical bond theory, and the following molecular formula was obtained:

$$LiMgPO_4=Li(Mg/Zn/Ni)PO(1)O(2)2O(3)$$

$$=Li_{1/3}O(1)_{1/2}+Li_{1/3}O(2)_{1/2}+Li_{1/3}O(3)_{1/2}+(Mg/Zn/Ni)_{1/6}O(1)_{1/4}+(Mg/Zn/Ni)_{1/6}O(2)_{1/4}+(Mg/Zn/Ni)_{1/3}O(3)^1{}_{1/2}+(Mg/Zn/Ni)/3O(3)^2{}_{1/2}+P_{1/4}O(1)_{1/4}+P_{1/4}O(2)_{1/4}+P_{1/2}O(3)_{1/2}$$

According to the decomposition formula, the chemical bonds and related bond energy are obtained and listed in Table S3. It can be seen from Table S3 that the trend of total lattice energy U is consistent with that of P-O bond energy. Combined with ρ_r plot and $Q\times f$ values, the change of Li-O bond energy is negatively correlated with the change of $Q\times f$ value, indicating that the increase of Li-O inhibits the increase of $Q\times f$ value. Mg-O bond is related to the stability of sintering properties. The Mg-O lattice energy of x = 0.04, x = 0.05 and x = 0.06 deviates far from 3400eV. The ρ_r of these component points is basically unchanged in the sintering range of 850-950°C, indicating that Mg-O bond controls the sensitivity of sintering properties to temperature. P-O bond has a great correlation with $Q\times f$ value, and its variation trend is basically consistent

with $Q\times f$ value. Further detailed analysis of three P-O bonds shows that the change trend of P-O (2) is closer to that of $Q\times f$ value, as plotted in Fig. S3 and Fig. S4.

Bond energy reflects the strength of chemical bond to a certain extent and is an important reference for crystal thermal stability. It is generally expressed by the energy required for chemical bond fracture. The bond energy of chemical bond can be calculated (Formula S1-S5) according to the chemical bond and electronegativity theory proposed by Sanderson [35]. The calculation results are shown in Table S4. The average bond energy of $LiMg_{0.9}Zn_{0.1-x}Ni_xPO_4$ ceramics is plotted in Fig. 5(a). When $x = 0$, the average bond energy is 248.6 kJ/mol, reaching the maximum of 250.22 kJ/mol with $x = 0.04$. Then the bond energy decreases with further increasing x, which is consistent with the trend of τ_f value of $LiMg_{0.9}Zn_{0.1-x}Ni_xPO_4$ ceramics. The bond energy of P-O bond, which also reaches a maximum of 1477.47 kJ/mol at x=0.04 and then decreases and tends to be stable. Fig. 5(b) shows the average bond energies of three Li-O bonds, four Mg-O bonds and three P-O bonds for $LiMg_{0.9}Zn_{0.1-x}Ni_xPO_4$ ceramics. It is clear that P-O bond plays a dominant role in τ_f value in $LiMg_{0.9}Zn_{0.1-x}Ni_xPO_4$ ceramics.

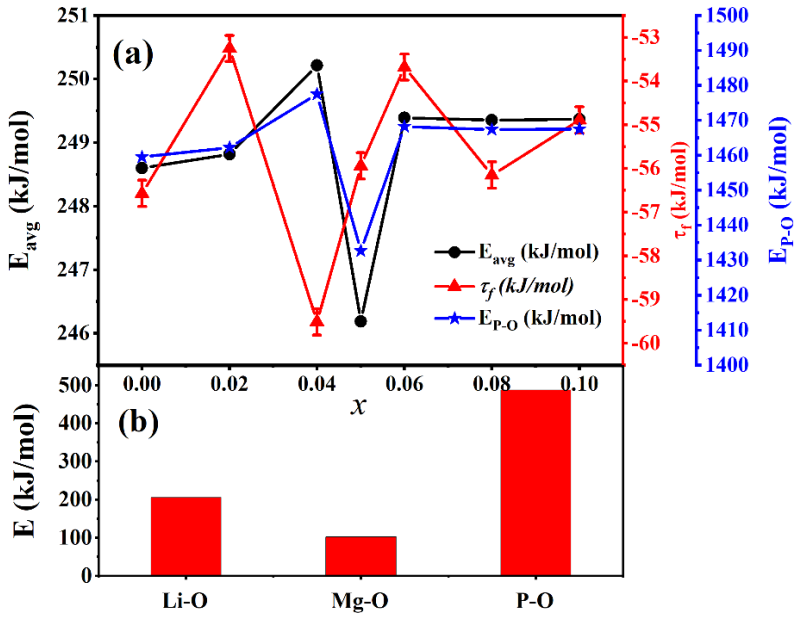

Fig. 5 (a) The values of τ_f, average bond energy E_{avg} and P-O bond energy E_{P-O} in $LiMg_{0.9}Zn_{0.1-x}Ni_xPO_4$ ceramics as a function of x; (b) the corresponding average bond energy of Li-O, Mg-O and P-O

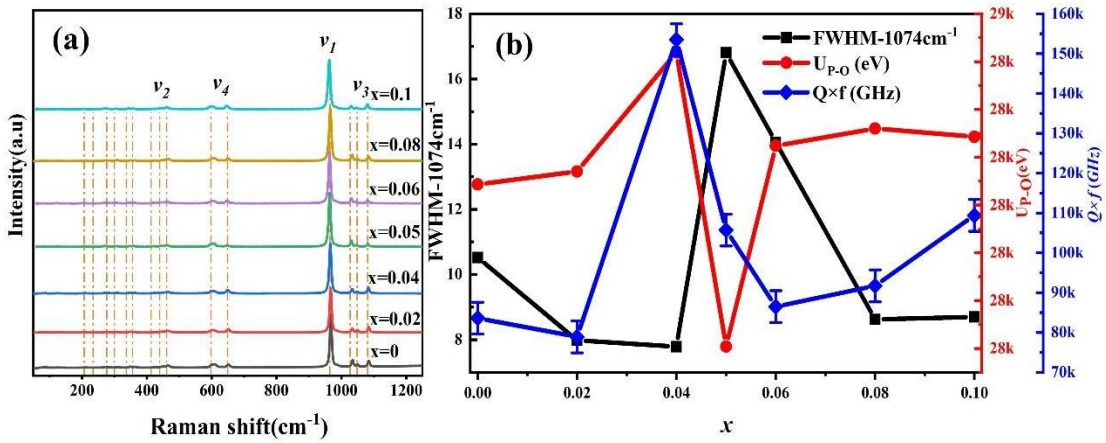

Fig. 6 (a) Raman spectra, and (b) FWHM, U_{P-O} and $Q\times f$ at 1074cm^{-1} of $LiMg_{0.9}Zn_{0.1-x}Ni_xPO_4$ ceramics as a function of x.

The internal lattice vibration of microwave dielectric ceramics is related to the crystal structure and inherent properties of ceramics. Raman spectroscopy and infrared reflection spectroscopy are effective means to study lattice vibration characteristics and inherent dielectric properties [36]. It is found that the $LiMg_{0.9}Zn_{0.1-x}Ni_xPO_4$ ceramics

share 48 Raman active modes ($LiMg_{0.9}Zn_{0.06}Ni_{0.04}PO_4$: $\Gamma = 15A_g + 9B_{1g} + 15B_{2g} + 9B_{3g}$). The Raman spectra of $LiMg_{0.9}Zn_{0.1-x}Ni_xPO_4$ ceramics are shown in Fig. 6(a), which exhibit 21-23 external modes (< 400 cm^{-1}, 100-250cm^{-1} are vibrations of Zn-O bonds, 338 and 352 cm^{-1} are stretching vibrations of Li-O), and 21-23 internal modes (> 400 cm^{-1}, bending vibration of O-Li-O: 424 cm^{-1}; bending vibration of O-Li-O, bending vibration of O-P-O: v_2 = 416-468 cm^{-1}; [NiO_6] bending vibration and P vibration: v_4 =590-650 cm^{-1}; P-O stretching vibration: v_1=958cm^{-1}, v_3=1020-1080 cm^{-1}). Raman characteristic peak half width (FWHM) of crystals can be used to characterize the degree of crystallization and the stress relationship. High purity crystals will cause the narrow down of FWHM value, and vice versa. Fig. 6(b) shows the relationship between microwave dielectric properties and FWHM of $LiMg_{0.9}Zn_{0.1-x}Ni_xPO_4$ ceramics at 1074cm^{-1}. It can be found that the change of FWHM shows an opposite trend to that of the lattice energy of P-O (U_{P-O}). When FWHM increases, U_{P-O} decreases, which indicates that the change of FWHM is inversely proportional to that of $Q \times f$.

Infrared reflection spectrum is commonly used to characterize the intrinsic dielectric response of the system. To reveal the influence of Zn and Ni composite substitution on the related microwave dielectric properties, the infrared reflection spectrum has been carried out and fitted with a four-parameter semi-quantum model (4-P). Fig. 7(a) and Fig. 7(d) show the room temperature infrared reflection spectra of $LiMg_{0.9}Zn_{0.1}PO_4$ and $LiMg_{0.9}Zn_{0.06}Ni_{0.04}PO_4$, respectively. 12 vibration modes are observed in the infrared reflection spectra of $LiMg_{0.9}Zn_{0.1}PO_4$ and $LiMg_{0.9}Zn_{0.06}Ni_{0.04}PO_4$ phases, while there should be 35 and 45 vibration modes in

$LiMg_{0.9}Zn_{0.1}PO_4$ structure according to the group theory analysis. These unobserved vibration modes may be too weak or covered by stronger and wider vibration modes. Fig. 7 shows the test spectra, 4-P fitting spectra and the real and imaginary parts of the complex permittivity corresponding to K-K transformation of $LiMg_{0.9}Zn_{0.1}PO_4$ and $LiMg_{0.9}Zn_{0.06}Ni_{0.04}PO_4$ infrared reflectance spectra. It can be seen that the spectral lines obtained by the 4-P fitting method and the K-K calculation method coincide well, indicating that the fitting results are effective and reliable. Table S5 and Table S6 show the dispersion parameters obtained by fitting $LiMg_{0.9}Zn_{0.1}PO_4$ and $LiMg_{0.9}Zn_{0.06}Ni_{0.04}PO_4$, with ε_{cal}=6.73, $\tan\delta_{cal}$=7.554×10^{-5} and ε_{cal}=6.19, $\tan\delta_{cal}$=6.8143×10^{-5}, respectively.

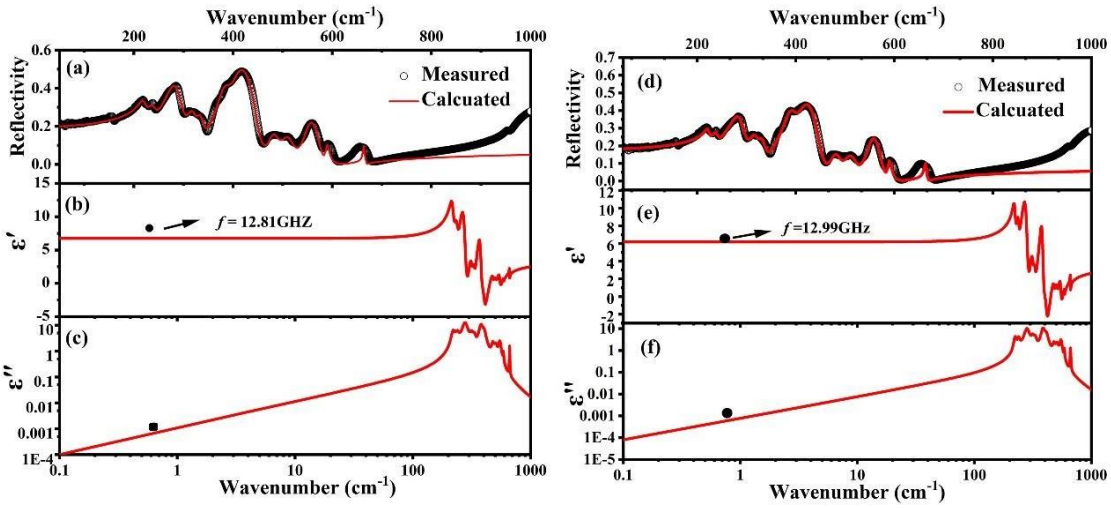

Fig. 7 (a) (d) measured and fitted infrared reflectance spectrum; (b) (e) real part obtained by K-K fitting; (c) (f) imaginary part obtained by K-K fitting.

4. Conclusions

In this work, $LiMg_{0.9}Zn_{0.1-x}Ni_xPO_4$ (x=0-0.1) microwave dielectric ceramics were prepared by a solid-state sintering route. XRD patterns of $LiMg_{0.9}Zn_{0.1-x}Ni_xPO_4$

ceramics confirmed the formation of a single phase without detection of any secondary phases. The lattice parameters, densification, and microstructure have been significantly affected by changing Zn/Ni ratio. The optimum properties were obtained at a ratio of (Zn/Ni=3/2), at a sintering temperature of 875℃. The influences of the intrinsic factors on the microwave dielectric properties of $LiMg_{0.9}Zn_{0.1-x}Ni_xPO_4$ ceramics were studied by P-V-L theory. It was found that the ε_r of ceramics was mainly affected by the ionic polarizability. The lattice energy of P-O bond was much larger than that of Mg-O bond and Li-O bond, playing a decisive role in the $Q\times f$ of ceramics. The value of τ_f was mainly affected by the bond energy, where the P-O bond showed the highest bond energy and a major contribution to τ_f. The optimal composition of $LiMg_{0.9}Zn_{0.06}Ni_{0.04}PO_4$ exhibited excellent microwave dielectric performance of $Q\times f$~ 153,500GHz, ε_r ~ 7.13 and τ_f ~ -59ppm/℃, which makes it a promising candidate for LTCC application.

Acknowledgements

This work was supported by the National Natural Science Foundation of China under Grant No. 52161145401, and No.51672063. The authors gratefully also acknowledge the financial support from Guangdong Key Platform & Programs of the Education Department of Guangdong Province for funding (2021ZDZX1003), Guangdong Provincial Key Laboratory (2014B030301014) and the Construction of Basic Research Institutions from Shenzhen Science, Technology and Innovation Commission.

References

[1] W. C. Lou, M. M. Mao, K. X. Song, K. W. Xu, B. Liu, W. J. Li, B. Yang, Z. M. Qi, J. W. Zhao, S. K. Sun, H. X. Lin, Y. Y. Hu, D. Zhou, D. W. Wang, I. M. Reaney, Low permittivity cordierite-based microwave dielectric ceramics for 5G/6G telecommunications, J. Eur. Ceram. Soc. 42 (2022) 2820-2826.

[2] J. H. Lee, G. DeJean, S. Sarkar, S. Pinel, K. Lim, J. Papapolymerou, J. Laskar, M. M. Tentzeris, Highly integrated millimeter-wave passive components using 3-D LTCC system-on-package (SOP) technology, IEEE Trans. Microw. Theory Techn. 53 (2005) 2220-2229.

[3] D. Agrawal, Latest global developments in microwave materials processing, Mater. Res. Innov. 14 (2010) 3-8.

[4] Y. H. Yang, Y. L. Wu, Z. Zhuang, M. D. Kong, W. M. Wang, C. Wang, An ultraminiaturized bandpass filtering Marchand balun chip with spiral coupled lines based on GaAs integrated passive device technology, IEEE Plasma Sci. 48 (2020) 3067-3075.

[5] F. Shi, H. L. Dong, Correlation of crystal structure, dielectric properties and lattice vibration spectra of $(Ba_{1-x}Sr_x)(Zn_{1/3}Nb_{2/3})O_3$ solid solutions, Dalton Trans. 40 (2011) 6659-6667.

[6] T. Zhou, Y. H. Liu, K. X. Song, L. Y. Xue, P. Xu, A. Khesro, D. W. Wang, B. Liu, M. M. Mao, F. Shi, S. K. Sun, New low- ε_r, temperature stable $Mg_3B_2O_6$-$Ba_3(VO_4)_2$ microwave composite ceramic for 5G application, J. Am. Ceram. Soc. 104 (2021) 3818-3822.

[7] A. Goulas, G. Chi-Tangyie, D. W. Wang, S. Y. Zhang, A. Ketharam, B. L. Vaidhyanathan, I. M. Reaney, D. A. Cadman, W. G. Whittow, J. C. Vardaxoglou, D. S. Engstrøm, Additively manufactured ultra-low sintering temperature, low loss $Ag_2Mo_2O_7$ ceramic substrates, J. Eur. Ceram. Soc. 41 (2021) 394-401.

[8] A. Goulas, G. Chi-Tangyie, D. W. Wang, S. Y. Zhang, A. Ketharam, B. L. Vaidhyanathan, I. M. Reaney, D. A. Cadman, W. G. Whittow, J. C. Vardaxoglou, D. S. Engstrøm, Microstructure and microwave dielectric properties of 3D printed low loss $Bi_2Mo_2O_9$ ceramics for LTCC applications, Appl. Mater. Today. 21 (2020) 100862.

[9] Y. B. Guo, J. T. Ma, J. X. Zhao, K. Du, Z. T. Fang, Y. Q. Zheng, W. Z. Lu, W. Lei, Low-temperature sintering and microwave dielectric properties of $CaSn_xSiO_{(3+2x)}$-based positive τ_f compensator, Ceram. Int. 44 (2018) 18209-18212.

[10] B. K. Choi, S. W. Jang, E. S. Kim, Dependence of microwave dielectric properties on crystallization behavior of $CaMgSi_2O_6$ glass-ceramics, Mater. Res. Bull. 67 (2015) 234-238.

[11] X. Q. Song, K. Du, J. Li, X. K. Lan, W. Z. Lu, X. H. Wang, W. Lei, Low-fired fluoride microwave dielectric ceramics with low dielectric loss, Ceram. Int. 45 (2019) 279-286.

[12] Y. J. Gu, X. H. Yang, X. Wang, J. L. Huang, Q. Li, L. H. Li, X. L. Li, B. H. Kim, Low temperature sintering and dielectric properties of Li_2MgTiO_4 microwave ceramics with $BaCu(B_2O_5)$ addition for LTCC applications, J. Mater. Sci.: Mater. Electron. 30 (2019) 18025-18030.

[13]R. Peng, Y. X. Li, G. L. Yu, Y. C. Lu, S. Li, Effect of Co^{2+} substitution on the microwave dielectric properties of $LiZnPO_4$ ceramics, J. Electron. Mater. 47 (2018) 7281-7287.

[14]Z. F. Cheng, X. Hu, Y. Li, Z. Y. Ling, Fabrication and microwave dielectric properties of Mg_2SiO_4-$LiMgPO_4$-TiO_2 composite ceramics, J. Am. Ceram. Soc. 99 (2016) 2688-2692.

[15]C. C. Xia, D. H. Jiang, G. H. Chen, Y. Lou, B. Li, C. L. Yuan, C. R. Zhou, Microwave dielectric ceramic of $LiZnPO_4$ for LTCC applications, J. Mater. Sci.: Mater. Electron. 28 (2017) 12026-12031.

[16]X. Hu, Z. F. Cheng, Y. Li, Z. Y. Ling, Dielectric relaxation and microwave dielectric properties of low temperature sintering $LiMnPO_4$ ceramics, J. Alloys Compd. 651 (2015) 290-293.

[17]P. Zhang, S. X. Wu, M. Xiao, The microwave dielectric properties and crystal structure of low temperature sintering $LiNiPO_4$ ceramics, J. Eur. Ceram. Soc. 38 (2018) 4433-4439.

[18]Y. Lv, R. Z. Zuo, Y. Cheng, C. Zhang, Low - Temperature Sinterable $(1-x)Ba_3(VO_4)_2$–$xLiMg_{0.9}Zn_{0.1}PO_4$ Microwave Dielectric Ceramics, J. Am. Ceram. Soc. 96 (2013) 3862-3867.

[19]E. C. Xiao, Z. K. Cao, J. Z. Li, X. H. Li, M. T. Liu, Z. X. Yue, Y. Chen, G. H. Chen, K. X. Song, H. F. Zhou, F. Shi, Crystal structure, dielectric properties, and lattice vibrational characteristics of $LiNiPO_4$ ceramics sintered at different temperatures, J. Am. Ceram. Soc. 103 (2020) 2528-2539.

[20]D. W. Wang, J. R. Chen, G. Wang, Z. L. Lu, S. K. Sun, J. L. Li, J. Jiang, D. Zhou, K. X. Song, L. M. Reaney, Cold sintered $LiMgPO_4$ based composites for low temperature co-fired ceramic (LTCC) applications, J. Am. Ceram. Soc. 103. (2020) 6237-6244.

[21]D. Thomas, M. T. Sebastian, Temperature-compensated $LiMgPO_4$: a new glass-free low-temperature cofired ceramic, J. Am. Ceram. Soc. 93 (2010) 3828-3831.

[22]D. Thomas, M. T. Sebastian, Effect of Zn^{2+} substitution on the microwave dielectric properties of $LiMgPO_4$ and the development of a new temperature stable glass free LTCC, J. Eur. Ceram. Soc. 32 (2012) 2359-2364.

[23]Z. W. Dong, Y. Zheng, P. Cheng, X. P. Lv, W. Y. Zhang, W. Zhou, W. H. Xiong, Preparation and microwave dielectric properties of $Li(Mg_{1-x}Co_x)PO_4$ ceramics for low-temperature cofired ceramic applications, Ceram. Int. 40 (2014) 14865-14869.

[24]Z. W. Dong, Y. Zheng, P. Cheng, X. P. Lv, W. Zhou, Microwave dielectric properties of $Li(Mg_{1-x}Ni_x)PO_4$ ceramics for LTCC applications, Ceram. Int. 40 (2014) 12983-12988.

[25]P. Zhang, K. X. Sun, S. X. Wu, M. Xiao, Microwave dielectric properties of low temperature co-fired ceramics $LiMg_{1-x}A_xPO_4$ (A=Mn, Ca, $0.02 \leq x \leq 0.08$), Mater. Lett. 255 (2019) 126565.

[26]H. W. Chen, H. Su, H. W. Zhang, T. C. Zhou, B. W. Zhang, J. F. Zhang, X. L. Tang, Low-temperature sintering and microwave dielectric properties of $(Zn_{1-x}Co_x)_2SiO_4$ ceramics, Ceram. Int. 40 (2014) 14655-14659.

[27]C. J. Pei, J. J. Tan, Y. Li, G. G. Yao, Y. M. Jia, Z. Y. Ren, P. Liu, H. W. Zhang,

Effect of Sb-site nonstoichiometry on the structure and microwave dielectric properties of $Li_3Mg_2Sb_{1-x}O_6$ ceramics, J. Adv. Ceram. 9 (2020) 588-594.

[28]X. Zhou, L. T. Lin, J. J. Sun, N. K. Zhang, H. Z. Sun, H. T. Wu, W. H. Tao, Effects of $(Mg_{1/3}Sb_{2/3})^{4+}$ substitution on the structure and microwave dielectric properties of $Ce_2Zr_3(MoO_4)_9$ ceramics, J. Adv. Ceram. 10 (2021) 778-789.

[29]R. Xiang, H. Su, Q. Zhang, Y. X. Li, X. L. Tang, Crystal structure and improved microwave dielectric properties of $ZnZr_{(1-x)}Ti_xNb_2O_8$ ceramics, J. Mater. Sci.: Mater. Electron. 31 (2020) 4769-4779.

[30]C. Xing, J. Z. Li, J. Wang, H. L. Chen, H. Y. Qiao, X. Q. Yin, Q. Wang, Z. M. Qi, F. Shi, Internal relations between crystal structures and intrinsic properties of nonstoichiometric $Ba_{1+x}MoO_4$ ceramics, Inorg. Chem. 57 (2018) 7121-7128.

[31]F. Y. Huang, H. Su, Y. X. Li, H. W. Zhang, X. L. Tang, Low-temperature sintering and microwave dielectric properties of $CaMg_{1-x}Li_{2x}Si_2O_6$ (x=0−0.3) ceramics, J. Adv. Ceram. 9 (2020) 471-480.

[32]W. C. Lou, K. X. Song, F. Hussain, B. Liu, H. B. Bafrooei, H. X. Lin, W. T. Su, F. Shi, D. W. Wang, Bond characteristics and microwave dielectric properties of $(Li_{0.5}Ga_{0.5})^{2+}$ doped $Mg_2Al_4Si_5O_{18}$ ceramics, Ceram. Int. 46 (2020) 28631-28638.

[33]X. Q. Song, W. Z. Lu, Y. H. Lou, T. Chen, S. W. Ta, Z. X. Fu, W. Lei, Synthesis, lattice energy and microwave dielectric properties of $BaCu_{2-x}Co_xSi_2O_7$ ceramics, J. Eur. Ceram. Soc. 40 (2020) 3035-3041.

[34]C. Y. Cai, X. Q. Chen, H. Li, J. Xiao, C. W. Zhong, S. R. Zhang, Microwave dielectric properties of $Ca_{1-x}Sr_xMgSi_2O_6$ ceramics, Ceram. Int. 46 (2020) 27679-

27685.

[35]R. T. Sanderson, Electronegativity and bond energy, J. Am. Ceram. Soc. 105 (1983) 2259-2261.

[36]W. C. Lou, K. X. Song, F. Hussain, A. Khesro, J. W. Zhao, H. B. Bafrooei, T. Zhou, B. Liu, M. M. Mao, K. W. Xu, E. Taheri-nassaj, D. Zhou, S. J. Lou, S. K. Sun, H. X. Lin, D. W. Wang, Microwave dielectric properties of $Mg_{1.8}R_{0.2}Al_4Si_5O_{18}$(R = Mg, Ca, Sr, Ba, Mn, Co, Ni, Cu, Zn) cordierite ceramics and their application for 5G microstrip patch antenna, J. Eur. Ceram. Soc. 42 (2022) 2254-2260.

Table S1 The average radius of complex Zn^{2+}-Ni^{2+} as a function of Zn/Ni Ratio

Zn/Ni Ratio	Zn(0.74Å) Content	Ni(0.69Å) Content	Zn/Ni(Å) Average ionic radius
-	1	0	0.74
4:1	0.8	0.2	0.73
3:2	**0.6**	**0.4**	**0.72(Mg^{2+})**
1:1	0.5	0.5	0.715
2:3	0.4	0.6	0.71
1:4	0.2	0.8	0.7
-	0	1	0.69

Table S2 $LiMg_{0.9}Zn_{0.1-x}Ni_xPO_4$ unit cell parameter table ($0 \leq x \leq 0.1$)

$LiMg_{0.9}Zn_{0.1-x}Ni_xPO_4$							
x	0	0.02	0.04	0.05	0.06	0.08	0.1
a(Å)	10.1406	10.12953	10.14018	10.12953	10.13739	10.1386	10.1324
b(Å)	5.9055	5.90405	5.90913	5.90405	5.90858	5.9092	5.90470
c(Å)	4.6925	4.68992	4.69266	4.68992	4.69191	4.6930	4.69130
α=β=γ(°)	90	90	90	90	90	90	90
V($Å^3$)	281.006	280.673	281.182	280.705	281.034	281.162	280.673
ρ_t(g/cm^3)	3.073	3.074	3.079	3.101	3.077	3.127	3.068
Rωp	8.15	4.98	7.18	6.19	4.82	6.14	3.34
Rp	5.64	3.49	5.24	4.53	6.65	4.32	4.79

χ^2	3.45	4.30	3.79	2.42	3.76	4.65	4.45

Table S3 The lattice energy in $LiMg_{0.9}Zn_{0.1-x}Ni_xPO_4$

Chemical bond	$LiMg_{0.9}Zn_{0.1-x}Ni_xPO4$ Lattice energy $U_{(eV)}$						
	x=0	x=0.02	x=0.04	x=0.05	x=0.06	x=0.08	x=0.1
Li-O(1)	312.23	312.50	313.45	313.81	312.92	312.13	311.61
Li-O(2)	325.05	324.72	323.85	323.67	325.13	324.42	325.62
Li-O(3)	314.61	314.44	315.03	315.36	315.76	315.10	315.06
Mg(Zn\Ni)-O(1)	560.29	560.91	559.15	554.36	560.80	563.73	565.16
Mg(Zn\Ni)-O(2)	580.34	579.76	577.52	597.22	575.26	578.3	575.33
Mg(Zn\Ni)-O(3)[1]	1160.42	1160.38	1153.15	1172.03	1150.98	1160.48	1161.11
Mg(Zn\Ni)-O(3)[2]	1099.20	1098.99	1099.08	1086.05	1100.54	1099.26	1098.10
P-O(1)	7030.89	7089.34	7136.60	7032.37	7122.71	7099.01	7098.15
P-O(2)	7083.40	7049.07	7109.09	6822.02	7069.19	7068.434	7077.85
P-O(3)	14029.05	14031.92	14173.15	13949.65	14031.77	14092.77	14066.70
A$U_{\text{Li-O}}$	951.95	951.66	952.35	952.85	953.81	951.65	952.29
A$U_{\text{Mg(Zn\Ni)-O}}$	3400.26	3400.02	3388.90	3409.67	3387.58	3401.80	3399.70
A$U_{\text{P-O}}$	28143.34	28170.33	28418.83	27804.04	28223.66	28260.21	28242.71
AU	32495.55	32522.02	32760.08	32166.56	32565.06	32613.65	32594.70
AvgU	3249.56	3252.20	3276.01	3216.66	3256.51	3261.37	3259.47

Table S4 Bond energy of $LiMg_{0.9}Zn_{0.1-x}Ni_xPO_4$ ceramics ($0 \leq x \leq 0.1$)

	Bond energy ***E*** (kJ/mol)						
Bond type	x = 0	x = 0.02	x = 0.04	x = 0.05	x = 0.06	x = 0.08	x = 0.1

Li-O(1)	202.27	202.34	203.02	203.23	202.77	202.03	201.76
Li-O(2)	210.19	209.94	209.49	209.36	210.37	209.66	210.47
Li-O(3)	203.70	203.55	204.01	204.20	204.54	203.87	203.91
Mg(Zn\Ni)-O(1)	100.99	101.12	100.67	99.74	101.00	101.71	102.00
Mg(Zn\Ni)-O(2)	105.27	105.14	104.58	108.91	104.07	104.83	104.17
Mg(Zn\Ni)-O(3)[1]	105.24	105.23	104.37	106.49	104.12	105.24	105.29
Mg(Zn\Ni)-O(3)[2]	98.73	98.71	98.64	97.35	98.78	98.73	98.60
P-O(1)	484.78	492.84	496.21	490.14	497.13	493.11	493.24
P-O(2)	492.33	487.03	492.23	460.75	489.34	488.70	490.30
P-O(3)	482.47	482.35	489.02	481.79	481.79	485.57	483.97
AE_{Li-O}	616.17	615.83	616.52	616.79	617.67	615.57	616.14
$AE_{Mg(Zn\backslash Ni)-O}$	410.23	410.23	408.26	412.48	407.97	410.52	410.06
AE_{P-O}	1459.58	1462.22	1477.47	1432.68	1468.26	1467.38	1467.51
AE	2485.98	2488.25	2502.25	2461.95	2493.91	2493.46	2493.71
E_{avg}	248.6	248.82	250.22	246.19	249.39	249.353	249.37

Table S5 The dispersion parameters of $LiMg_{0.9}Zn_{0.1}PO_4$ ceramics obtained by fitting

Mode	ω_{oj}	ω_{pj}	γ_j	$\triangle\varepsilon_j$	$\tan\delta_j\times10^{-4}$
1	220.44	131.45	16.884	0.356	0.0766
2	238.64	131.56	19.883	0.304	0.0833
3	278.3	326.24	32.195	1.37	0.116
4	316.43	153.22	22.6	0.234	0.0714
5	333.28	113.21	16.402	0.115	0.0492
6	379.29	311.83	29.945	0.676	0.0789
7	402.56	256.79	35.088	0.407	0.0872
8	478.64	134.02	26.514	0.0784	0.0554
9	506.64	146.83	33.532	0.084	0.0662
10	548.18	183.56	29.206	0.112	0.0533
11	587.67	50.535	7.3546	0.00739	0.0125
12	663.7	65.423	3.6318	0.00972	0.00547

$LiMg_{0.9}Zn_{0.1}PO_4$	ε_∞ = 2.98	ε_0 = 3.75	ε_{cal}=6.73	$\tan\delta_{cal}$=7.554×10^{-5}

Table S6 The dispersion parameters of $LiMg_{0.9}Zn_{0.06}Ni_{0.04}PO_4$ ceramics obtained by fitting

Mode	ω_{oj}	ω_{pj}	γ_j	$\triangle\varepsilon_j$	$\tan\delta_j$×10^{-4}
1	223.02	88.633	10.771	0.158	0.0483
2	239.13	96.543	14.239	0.163	0.0595
3	281.84	282.85	29.579	1.01	0.105
4	315.93	142.97	20.936	0.205	0.0663
5	331.6	123.04	18.391	0.138	0.0555
6	386.03	309.21	27.718	0.642	0.0718
7	411.01	270.22	36.313	0.432	0.0884
8	478.86	137.83	25.91	0.0828	0.0541
9	508.8	158.96	31.718	0.0976	0.0623
10	549.16	199.63	26.937	0.132	0.0491
11	588.04	60.588	7.9584	0.0106	0.0135
12	662.76	77.562	5.056	0.0137	0.00763
$LiMg_{0.9}Zn_{0.06}Ni_{0.04}PO_4$	ε_∞ = 3.11	ε_0 =3.08	ε_{cal}=6.19	$\tan\delta_{cal}$=6.8143×10^{-5}	